University of Groningen

Surface curvature in triply-periodic minimal surface architectures as a distinct design parameter in preparing advanced tissue engineering scaffolds

Blanquer, Sebastien B. G.; Werner, Maike; Hannula, Markus; Sharifi, Shahriar; Lajoinie, Guillaume P. R.; Eglin, David; Hyttinen, Jari; Poot, Andre A.; Grijpma, Dirk W.

Published in:
Biofabrication

DOI:
10.1088/1758-5090/aa6553

IMPORTANT NOTE: You are advised to consult the publisher's version (publisher's PDF) if you wish to cite from it. Please check the document version below.

Document Version
Publisher's PDF, also known as Version of record

Publication date:
2017

Link to publication in University of Groningen/UMCG research database

Citation for published version (APA):
Blanquer, S. B. G., Werner, M., Hannula, M., Sharifi, S., Lajoinie, G. P. R., Eglin, D., Hyttinen, J., Poot, A. A., & Grijpma, D. W. (2017). Surface curvature in triply-periodic minimal surface architectures as a distinct design parameter in preparing advanced tissue engineering scaffolds. *Biofabrication*, *9*(2), [025001]. https://doi.org/10.1088/1758-5090/aa6553

Copyright
Other than for strictly personal use, it is not permitted to download or to forward/distribute the text or part of it without the consent of the author(s) and/or copyright holder(s), unless the work is under an open content license (like Creative Commons).

The publication may also be distributed here under the terms of Article 25fa of the Dutch Copyright Act, indicated by the “Taverne” license. More information can be found on the University of Groningen website: https://www.rug.nl/library/open-access/self-archiving-pure/taverne-amendment.

Take-down policy
If you believe that this document breaches copyright please contact us providing details, and we will remove access to the work immediately and investigate your claim.

Downloaded from the University of Groningen/UMCG research database (Pure): http://www.rug.nl/research/portal. For technical reasons the number of authors shown on this cover page is limited to 10 maximum.

Biofabrication

RECEIVED
15 November 2016

REVISED
24 February 2017

ACCEPTED FOR PUBLICATION
8 March 2017

PUBLISHED
12 April 2017

PAPER

Surface curvature in triply-periodic minimal surface architectures as a distinct design parameter in preparing advanced tissue engineering scaffolds

Sébastien B G Blanquer[1,2,7], Maike Werner[1], Markus Hannula[3], Shahriar Sharifi[1,4], Guillaume P R Lajoinie[5], David Eglin[6], Jari Hyttinen[3], André A Poot[1] and Dirk W Grijpma[1,4]

[1] MIRA Institute for Biomedical Technology and Technical Medicine, Department of Biomaterials Science and Technology, Faculty of Science and Technology, University of Twente, 7500 AE Enschede, The Netherlands
[2] Institut Charles Gerhardt de Montpellier UMR5253 CNRS-UM-ENSCM—Equipe Ingénierie et Architectures Macromoléculaires, Université de Montpellier, F-34095 Montpellier, France
[3] Department of Electronics and Communications Engineering, Tampere University of Technology, FI-33720 Tampere, Finland
[4] Department of Biomedical Engineering, University Medical Centre Groningen, 9713 AV Groningen, The Netherlands
[5] MESA+ Institute for Nanotechnology and MIRA Institute for Biomedical Technology and Technical Medicine, Physics of Fluids Group, Faculty of Science and Technology, University of Twente, 7500 AE Enschede, The Netherlands
[6] AO Research Institute Davos, Switzerland
[7] Author to whom any correspondence should be addressed.

E-mail: sebastien.blanquer@umontpellier.fr

Keywords: triply-periodic minimal surface (TPMS), surface curvature, stereolithography, poly(trimethylene carbonate) (PTMC), tissue engineering scaffold

Supplementary material for this article is available online

Abstract

Reproduction of the anatomical structures and functions of tissues using cells and designed 3D scaffolds is an ongoing challenge. For this, scaffolds with appropriate biomorphic surfaces promoting cell attachment, proliferation and differentiation are needed. In this study, eight triply-periodic minimal surface (TPMS)-based scaffolds were designed using specific trigonometric equations, providing the same porosity and the same number of unit cells, while presenting different surface curvatures. The scaffolds were fabricated by stereolithography using a photocurable resin based on the biocompatible, biodegradable and rubber-like material, poly(trimethylene carbonate) (PTMC). A numerical approach was developed to calculate the surface curvature distributions of the TPMS architectures. Moreover, the scaffolds were characterized by scanning electron microscopy, micro-computed tomography and water permeability measurements. These original scaffold architectures will be helpful to decipher the biofunctional role of the surface curvature of scaffolds intended for tissue engineering applications.

Introduction

Scaffold design plays a major role in cell and tissue organization in tissue-engineered constructs. There is an increasing body of evidence that cells can sense and respond to surface curvature, thereby making it an intriguing scaffold functionality for tissue engineering purposes. Local tissue growth rate was shown to depend on the pore geometry. Tissue growth was investigated in channels of different geometries (with perimeters in the millimeter range) and it was shown that tissue growth increased with increasing concave curvatures while tissue growth was minimal on convex areas [1, 2]. Furthermore, other approaches demonstrated the effect of curved surfaces on cell migration. It was observed that cells actively migrated out of concave pits while they adhered and proliferated on convex structures [3]. Recently, it was shown that single cells show different attachment modes to concave and convex spherical substrates with diameters ranging from 250 μm ($\approx$2–3 times mesenchymal stem cell size) to 750 μm (much larger than cell size). Cells in concave spherical substrates showed an upward lift of the cell body and migrated faster compared to cells on flat or convex surfaces, while convex substrates led to a flattened cell morphology,

© 2017 IOP Publishing Ltd

nuclear deformation and promoted osteogenic differentiation [4]. In addition, it was recently shown that mouse T lymphocytes cultured on sinusoidal wavy structures preferentially migrated along grooves with the most concave surface curvature [5]. In view of the remarkable effect of curved surfaces on cell behavior, the availability of scaffolds containing highly controllable surface curvatures might contribute to scaffold design optimization for tissue reconstruction.

Triply-periodic minimal surfaces (TPMS) are mathematically defined surface curvatures, infinite and periodic in the 3D Euclidean space, making them interesting surfaces for highly controllable and homogeneous scaffold designs. Minimal surfaces are frequently encountered in nature and play an essential role in guiding chemical, biochemical and cellular processes. Minimal surfaces are present in the atomic organization of molecules [6] and the lipid bilayer of cellular membranes [7, 8]. They are also reported in the description of the domain morphology of self-assembled block copolymers and macromolecules [9–12]. The specific conformations of minimal surfaces allow understanding of phase behavior and structure-function relations.

The natural organization of minimal surface structures responds to the physical principle which governs the forms and motions of objects, the principle of free energy minimization. In nature and man-made environments, systems normally try to arrange themselves to reduce their potential energy in order to consume less energy and increase their stability [13]. The term 'minimal surface' is directly linked to the surface energy and represents the lowest possible potential energy that a surface can have if its energy is proportional to the surface area. In consequence, structures that respect this configuration will be thermodynamically stable. The minimization of the surface energy leads automatically to typical curved structures with respect to the initial fixed boundary [14–16].

As TPMS structures adopt a periodic curved conformation, it seems relevant to investigate a new generation of tissue engineering scaffolds based on TPMS to emphasize the potential of surface curvature in tissue engineering. Surprisingly, besides the typical scaffolds with Gyroid [17] and Schwartz P architecture [18, 19], TPMS structures for tissue engineering applications have only been investigated as computational models [20–24]. Therefore, the aim of our work was to prepare a new library of mathematically designed tissue engineering scaffolds with sophisticated pore architecture based on TPMS. These complex scaffolds were built by stereolithography (SL), the most versatile rapid prototyping technique with the highest accuracy and precision to produce 3D structures at high resolution [17, 25–27]. Flexible and elastic scaffolds were prepared from a photo-curable resin based on reactive poly(trimethylene carbonate) (PTMC) oligomers which is recognized as biocompatible and bioerodible material [28]. The pore characteristics of the built scaffolds were investigated a.o. by micro-computed tomography (μCT) analysis as well as by determination of their water permeability. In addition, we developed a mathematical method to determine the surface curvature distribution for any type of TPMS structure which would be a more precise approach to define the porous features.

Materials and methods

Materials

Trimethylene carbonate (1,3-dioxan-2-one, TMC) was obtained from Foryou Medical, China. Stannous octoate (tin 2-ethylhexanoate, $SnOct_2$), trimethylolpropane (TMP), trimethylamine, methacrylic anhydride, hydroquinone, methanol absolute, anhydrous dichloromethane and propylene carbonate were purchased from Sigma-Aldrich, Germany. Lucirin TPO-L (ethyl 2,4,6-trimethylbenzoylphenyl phosphinate) was provided by BASF, Germany. Orasol Orange G was obtained from Ciba Specialty Chemicals, Switzerland. Reagents and solvents were of analytical grade and used as received.

Synthesis and characterization of macromer

Three-armed PTMC of 5000 g mol^{-1} was typically obtained by ring-opening polymerization. PTMC oligomer was prepared by polymerization of TMC (0.98 mol; 100 g) initiated by TMP (0.0196 mol, 2.62 g) and catalyzed by $Sn(Oct)_2$ (0.05 wt%), at 130 °C for 48 h under an argon atmosphere. The monomer conversion was determined by ^{1}H-NMR spectroscopy (Varian Innova 300 MHz, USA), using $CDCl_3$ as solvent.

End-functionalization of the PTMC oligomer was achieved by reacting hydroxyl end-groups with an excess of methacrylic anhydride (0.15 mol; 22 ml) in the presence of triethylamine (0.15 mol; 20 ml) in 100 ml of dry dichloromethane. The reaction was performed at room temperature under stirring and argon atmosphere for 5 d. The macromer was then isolated by precipitation in cold methanol. The degree of functionalization was determined by ^{1}H-NMR analysis in $CDCl_3$.

Stereolithography

A SL apparatus (EnvisionTec Perfactory Mini Multilens, Germany) equipped with a digital mirror device allowing projections of 1280 × 1024 pixels, each measuring 16 × 16 μm^2, was used to fabricate eight different TPMS scaffolds. The wavelength of the blue light irradiation ranged from 400 to 550 nm, with a peak at 440 nm. Mathematical formulas were developed and used to generate 3D structures using K3dSurf v0.6.2 software (freeware from http://k3dsurf.sourceforge.net). The generated structures were then modified to a volume of 10 × 10 × 10 mm^3 and

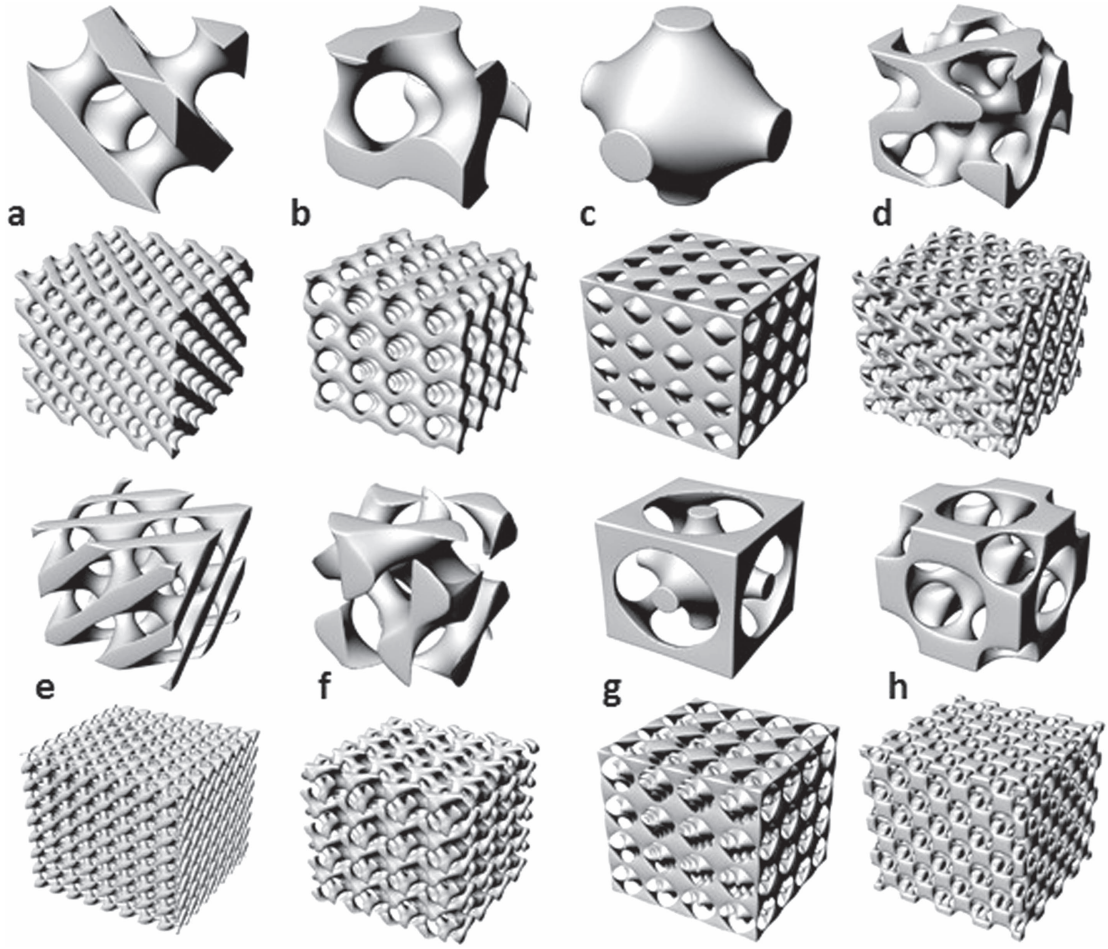

Figure 1. TPMS structures: (a) Diamond (D); (b) Gyroid (G); (c) Schwarz P (P); (d) Fischer–Koch S (S); (e) Double Diamond (DD); (f) Double Gyroid (DG); (g) Double Schwarz P (DP); (h) F-RD, for each structure the top design is one single unit cell and the bottom structure represents 4 × 4 × 4 unit cells.

converted into .stl files using computer-aided design software (Rhinoceros 3D, McNeel, Europe).

Resin formulation

Resin was prepared by diluting PTMC macromer in propylene carbonate (30 wt%), followed by mixing with Lucirin TPO-L initiator (5 wt% relative to the macromer) and Orasol Orange dye (0.15 wt% relative to the macromer). Using this resin, layers with a thickness of 25 μm were sequentially polymerized upon illumination for 50 s in the SL apparatus. After building, the scaffolds were carefully washed in acetone and ethanol.

Surface curvature

3D rendering of the structures and mapping of the curvatures were computed using Matlab (The MathWorks, Inc., Natick, MA, USA), according to the formula given in equation (1) (see below). Symbolic derivation was used to solve the equations and differentiate the expressions, except for two architectures (S and DG see figure 1 and table 1) that required a completely discretized numerical method.

The calculation of the Gaussian curvature distribution was implemented using the method described by Mackay *et al* [15]. The mathematical equations that approximate the typical surface of TPMS structures are expressed in the trigonometric function of x, y and z [29]. The trigonometric equations can be solved with regard to z, leading to a simplified expression [15, 18] for the surfaces in the form $F = \sum_i F_i(x, y)$. Hence, the Gaussian curvature K for each TPMS design can be expressed by the Laplace–Young equation (equation (1)), involving the first and second derivatives of the function

$$K_{\text{rad}}(x, y) = \frac{F_{xx}F_{yy} - F_{xy}F_{yx}}{(1 + F^2{}_x + F^2{}_y)^2}, \quad (1)$$

where the first and second derivatives are abbreviated as follows: $F_x = \frac{\partial F}{\partial x}$; $F_y = \frac{\partial F}{\partial y}$; $F_{xy} = \frac{\partial^2 F}{\partial x \partial y}$; $F_{xx} = \frac{\partial^2 F}{\partial x^2}$; $F_{yy} = \frac{\partial^2 F}{\partial y^2}$.

Each nodal equation presented in table 1, descriptive of a minimal surface, was correlated to its curvature computed using equation (1). The Gaussian curvature given by this equation can also be written as a function of the two non-dimensional local radii of curvature r_1 and r_2 as expressed in equation (2).

Table 1. Approximated periodic nodal equations for eight TPMS structures [24, 35].

TPMS structures	Nodal equations for TPMS: $f(x,y,z) = C$[a]	C
D (Diamond)	$\sin(x).\sin(y).\sin(z) + \sin(x).\cos(y).\cos(z) + \cos(x).\sin(y).\cos(z) + \cos(x).\cos(y).\sin(z) = C$	0.45
G (Gyroid)	$\cos(x).\sin(y) + \cos(y).\sin(z) + \cos(z).\sin(x) = C$	0.6
P (Schwarz P)	$\cos(x) + \cos(y) + \cos(z) = C$	0.67
S (Fischer–Koch S)	$\cos(2x).\sin(y).\cos(z) + \cos(2y).\sin(z).\cos(x) + \cos(2z).\sin(x).\cos(y) = C$	0.375
DD (Double Diamond)	$1.(\sin(2x).\sin(2y) + \sin(2y).\sin(2z) + \sin(2x).\sin(2z)) + 1.(\cos(2x).\cos(2y).\cos(2z)) = C$	0.35
DG (Double Gyroid)	$2.75.(\sin(2x).\sin(z).\cos(y) + \sin(2y).\sin(x).\cos(z) + \sin(2z).\sin(y).\cos(x))-1.(\cos(2x).\cos(2y) + \cos(2y).\cos(2z) + \cos(2z).\cos(2x)) = C$	0.95
DP (Double Schwarz P)	$0.5.(\cos(x).\cos(y) + \cos(y).\cos(z) + \cos(z).\cos(x)) + 0{,}2.(\cos(2x) + \cos(2y) + \cos(2z)) = C$	0
F-RD	$8.\cos(x).\cos(y).\cos(z) + 1.(\cos(2x).\cos(2y).\cos(2z)) - 1.(\cos(2x).\cos(2y) + \cos(2y).\cos(2z) + \cos(2z).\cos(2.x)) = C$	1.6

[a] Each TPMS scaffold has been designed as a periodic assembly 4π in all three dimensions of space (boundary condition $x, y, z = [-4\pi, 4\pi]$) for a volume of 10 × 10 × 10 mm.

$$K_{\text{rad}} = \frac{1}{r_1 r_2}. \quad (2)$$

Practically, the size and the repetition of the unit cells within the investigated scaffold are bound to vary in view of the specific tissue reconstruction targeted. Therefore, it is convenient to consider the bare equation given in table 1 and determine how the curvature will scale when changing the size of the unit cells, which allows to generalize the characterization of the surface curvature for any structure based on TPMS architecture.

$F(x)$ is considered as a direct solution of an equation from table 1, and $F_2(x)$ will be the scaled version of the TPMS architecture investigated. The structures being triply periodic, the unit cell is covered for $x \in \left[0, \frac{2\pi}{\omega}\right]$, i.e. $x_2 = \omega x \in [0, 2\pi]$ (and identically for y).

Here, we defined ω as $\omega = \frac{2\pi n}{m} = \frac{2\pi}{P_\pi}$, where $P_\pi = \frac{m}{n}$ and corresponds to the spatial period of the structure, n the number of unit cells along one side of the structure (which is fixed at 4 unit cells for the structures tested in this work) and m the size of the cubic structure in mm. Considering the new set of variables $\begin{cases} x_2 = \omega_x x \\ y_2 = \omega_y y \\ z_2 = \omega_z z \end{cases}$ and maintaining the aspect ratio results in $\omega_x = \omega_y = \omega_z$. Therefore the rescaled surface F_2 is now written as $\omega F_2(x, y) = F(\omega x, \omega y)$ leading to $\frac{\partial F_2}{\partial x}(x, y) = \frac{1}{\omega}\frac{\partial}{\partial x}(F(\omega x, \omega y)) = \frac{\partial F}{\partial x}(\omega x, \omega y)$, and similarly, $\frac{\partial^2 F_2}{\partial x^2}(x, y) = \frac{\partial}{\partial x}\left(\frac{\partial F(\omega x, \omega y)}{\partial x}\right) = \omega \frac{\partial^2 F}{\partial x^2}(\omega x, \omega y)$.

Finally, from equation (1) we can extract equation (3):

$$K_2(x, y) = \omega^2 K(x_2, y_2), \quad (3)$$

where K is the local Gaussian surface curvature.

The surface curvature distribution has been developed from only 90% of the surface area limit for each structure, as standard methods to describe distributions. This, is justified on the one hand by the fact the distributions tend to be mathematically infinite (or starting from 0), which renders errors bars useless in terms of statistical data interpretation. Furthermore, one needs to bear in mind that the extreme values of statistical distributions based on discrete data is intrinsically dependent on the chosen discretization step, and therefore do not carry any actual information on the system.

Scanning electron microscopy

Visualization of the built microsctructures was carried out by scanning electron microscopy (SEM, Philips XL 30 ESEM-FEG, The Netherlands) at an operating voltage of 5 kV, using pristine specimens sputter-coated with gold.

Micro-computed tomography

Structural analysis of the prepared scaffolds was performed by μCT scanning (MicroXCT-400 Carl Zeiss x-ray Microscopy, Pleasanton, USA) at an operating voltage of 60 kV and a tube current of 166 μA. Pixel size was 19.4 μm. Visualizations were done with Avizo (FEI Visualization Sciences Group). Porosities and pore size distributions were assessed with Fiji [30] program using BoneJ [31] plugin. Interconnectivity analysis for different pore sizes was also done with Matlab.

Scaffold permeability

Permeability was measured using a water flow set-up in the vertical direction [32, 33]. The principle was to let water flow through a scaffold and to collect the volume every 10 s for 10 min. A liquid tank was used to deliver the water at low pressures (25, 50 and 75 mbar). The permeability was determined by Darcy's law expressed in equation (4)

$$Q = \frac{A \cdot k \cdot \Delta P}{\mu \cdot L}, \quad (4)$$

where Q is the volumetric flow rate, A the surface area, k the intrinsic permeability, ΔP the pressure difference, μ the dynamic viscosity of water and L the thickness. The intrinsic permeability was determined from the slope c of the water flow (Q, measured in triplicate) versus ΔP using equation (5)

$$k = \frac{c \cdot \mu \cdot L}{A}. \quad (5)$$

Results

TPMS designs

Many 3D geometric architectures have been described as periodic minimal surfaces [34]. Among them, bicontinuous or biphasic TPMSs form a solid/void interface where the void space represents the pores of the 3D scaffold and the solid space is materialized by the polymer. The bicontinuous surfaces of TPMS structures are represented by complex harmonic equations. To allow analytical evaluation and fabrication, the harmonic equations were approximated by the periodic nodal surface [14]. Table 1 lists the approximated periodic nodal equations for eight TPMS structures [24, 35]. These equations allowed generating a CAD file, and extracting an STL file for use in the manufacturing by SL. By modulating a linear term (C) to the nodal equation, it is possible to define the pore characteristics and the surface curvature. Therefore, the role of the constant C can be defined as offsetting value increasing the volume fraction of the void space [24].

The investigated TPMS structures (table 1 and figure 1) have the capacity to yield stable 3D scaffolds, having a common porosity of 65% and a common number of 64 unit cells per scaffold, with a fixed cubic size of $m = 10$ mm.

As shown in figure 1, TPMS structures are periodic in three independent directions and can be infinitely reproduced by repetition of a cubic translational unit cell and thus might be used to construct a 3D porous scaffold. The bicontinuous geometry of TPMS structures gives a scaffold with total pore interconnectivity.

Schwarz P (P), Diamond (D) and Gyroid (G) geometries have been widely investigated from a mathematical perspective and are designed from catenoid and helicoid surfaces [36]. These structures were already proposed for tissue engineering scaffolds [17, 19]. Double Schwarz P (DP), Double Gyroid (DG), Double Diamond (DD), Fischer–Koch S (S) and F-RD are new geometries for tissue engineering applications, with varying surface curvature distributions through intertwined or interpenetrated surfaces. These structures present a high intrinsic complexity, moreover most of these new structures exhibit a high specific tortuosity which induce a relatively large surface area and would significantly increase the contact and the exchanges with the surfaces, which is required for cells adhesion. In addition, these 3D structures display specific and periodic surface curvatures.

Calculation of surface curvature

Although the definition of curvature is basically defined as the inverse of the radius of the curvature, in 3D the description of curvature is more complex. In 3D, at each point of the surface two different principal curvatures (k_1 and k_2) can be defined. Principal curvatures are used to calculate the mean curvature (H) and the Gaussian curvature (K) (table 2). For any type of minimal surface structure, at each point of the surface the principal curvatures have an equal magnitude but opposite sign, illustrating convex and concave shapes [29]. Therefore, the mean curvature (H), which is defined as the average of the principal curvatures (equation (6)), is equal to zero at any point of a TPMS structure. Gaussian curvature (K) is an intrinsic measure defined as the product of the principal curvatures (equation (7)). In contrast with the mean curvature, Gaussian curvature represents a local curvature within the structure.

Table 2. Expression of curvatures for minimal surfaces.

Mean curvature	$H = \frac{k_1+k_2}{2}$ (6)
Gaussian curvature	$K = k_1 \cdot k_2$ (7)
When $H = 0$, $k_1 = -k_2$	

As expressed in table 2, the mean curvature is at every point at the surface equal to zero ($H = 0$) for any type of minimal surface. Consequently, the Gaussian curvature varies in a periodic fashion with the curved trajectory along the surface, from a negative minimum value to a maximum value equal to zero on a flat surface.

In order to study the typical Gaussian curvature distribution of a specific TPMS scaffold, it is essential to fully define the surface curvature.

From equation (3), established in the Materials and methods section, the Gaussian curvature $|K|$ distributions were calculated for each TPMS function based on structures made with 4 unit cells in all three directions (n) and 10 mm length (m). The curvature mapping of each TPMS architecture was computed using equation (3) and presented in figure 2.

Scaffold designs based on TPMS display a defined periodic porous geometry with variation of the Gaussian curvatures. Therefore, several distinct variations of the Gaussian curvature can be obtained according to the type of TPMS architecture. Interestingly, besides the calculation of the curvature distribution, this method enables the determination of the number of unit cells (n) necessary to design a cubic or rectangular prism scaffold with a predefined size (m), required for a TPMS scaffold with desired Gaussian curvature values. This would allow for example, to investigate the influence of surface curvature on the behavior of seeded cells. In practice, it is essential to be able to vary the size of the scaffold according to the target application, which confirms the need to develop a method like this that allows a systematic determination of the curvature for any given TPMS scaffold.

Figure 3 reports the Gaussian curvature distribution numerically determined for the eight different TPMS scaffold designs calculated in mm^{-2}. The heterogeneity of the surface curvature distribution is

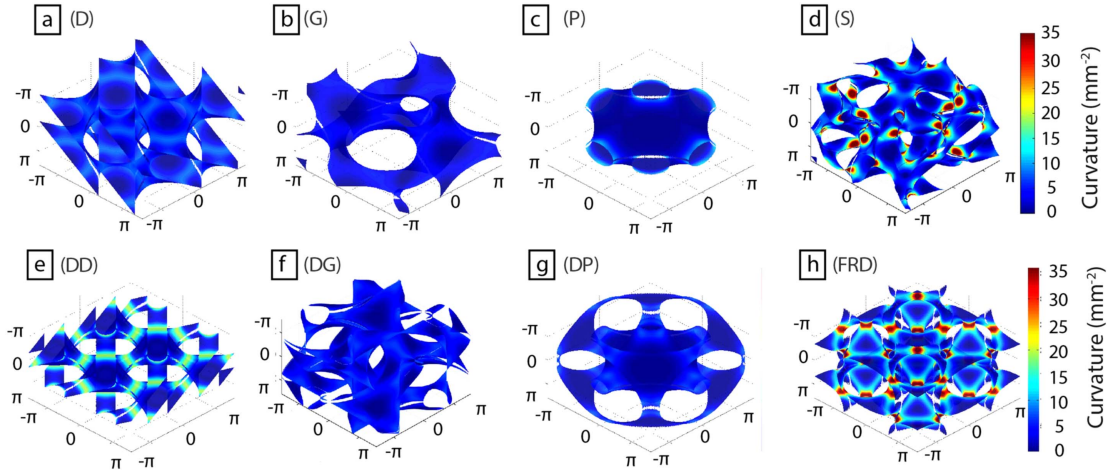

Figure 2. Gaussian curvature $|K|$ distribution along the surface of each TPMS structure. Color bars represent the Gaussian curvature values in mm^{-2}. (a) Diamond (D); (b) Gyroid (G); (c) Schwarz P (P); (d) Fischer–Koch S (S); (e) Double Diamond (DD); (f) Double Gyroid (DG); (g) Double Schwarz P (DP); (h) F-RD.

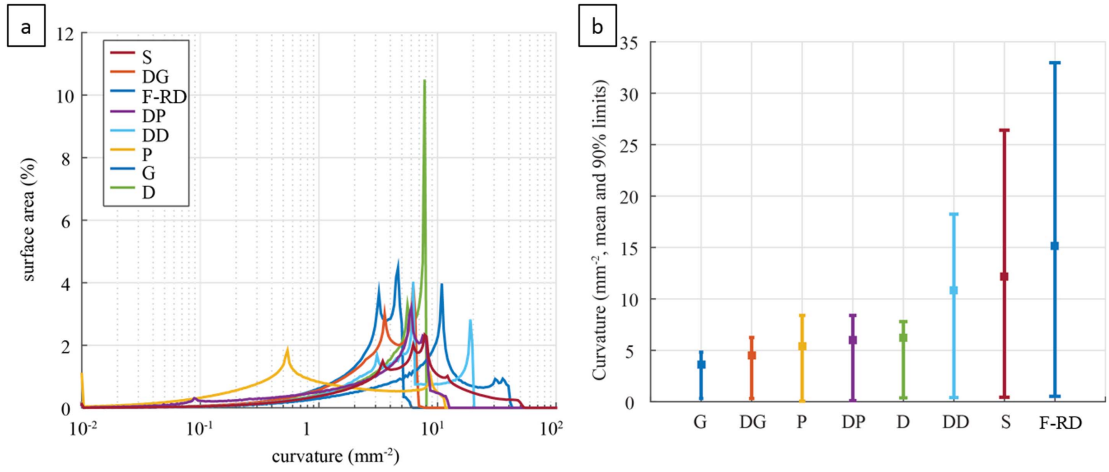

Figure 3. Complete distribution of the curvature in terms of surface area for each TPMS structures (a), and representation of the surface curvature distribution in histogram with the mean surface curvature distribution depicted by a square symbol and the full curvature distribution on 90% of the surface area limit is given by the interval bars.

clearly distributed on figure 3(a) which thus allows to emphasize the % of surface area dedicated to a specific surface curvature value. It is therefore clear that the TPMS structures can present several maxima in the % surface area at some values of the surface curvature. This aspect may be crucial for the creation of cell-supporting scaffolds since cell behavior is affected by the local curvature. To simplify these distributions, the figure 3(b) gives an idea of the mean curvature with the interval of surface curvature distributions for each structure.

The eight structures can be classified in two groups: G, DG, DP, P and D with relatively low surface curvatures and narrow curvature distributions, and DD, S and F-RD with substantially higher maximum surface curvatures and wide curvature distributions.

Fabrication of scaffolds with TPMS structures

Biodegradable PTMC oligomer was synthesized as previously described [37]. The monomer-to-initiator ratio was adjusted to obtain a molecular weight of 5000 g mol^{-1}. A high degree of acrylate functionalization of more than 95%, contributed to efficient photo-crosslinking by SL. A solution of 30 wt% of this low molecular weight macromer in propylene carbonate has a viscosity between 5 and 10 Pa s, which is well suited for manufacturing by SL. An optimized Orasol Orange dye concentration of 0.15 wt% relative to the macromer was used to control the penetration depth of the blue light and thus to avoid over-crosslinking between the printed layers. SEM images in supplementary information is available online at stacks.iop.org/BF/9/025001/mmedia show the typical layer-by-layer fabrication for the S structures.

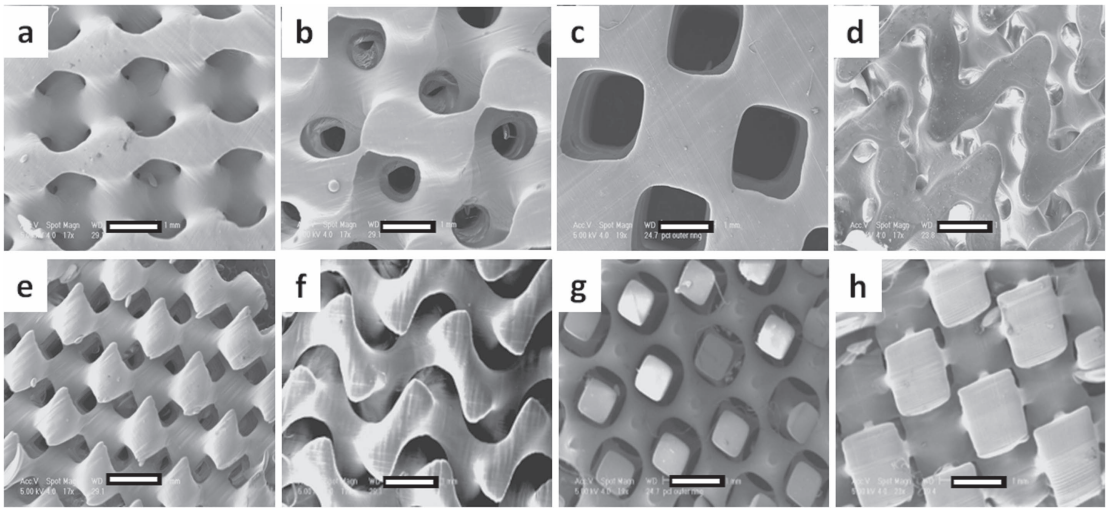

Figure 4. SEM visualization of the built TPMS scaffolds based on PTMC: (a) Diamond (D); (b) Gyroid (G); (c) Schwarz P (P); (d) Fischer–Koch S (S); (e) Double Diamond (DD); (f) Double Gyroid (DG); (g) Double Schwarz P (DP); (h) F-RD, (scale bars represent 1 mm).

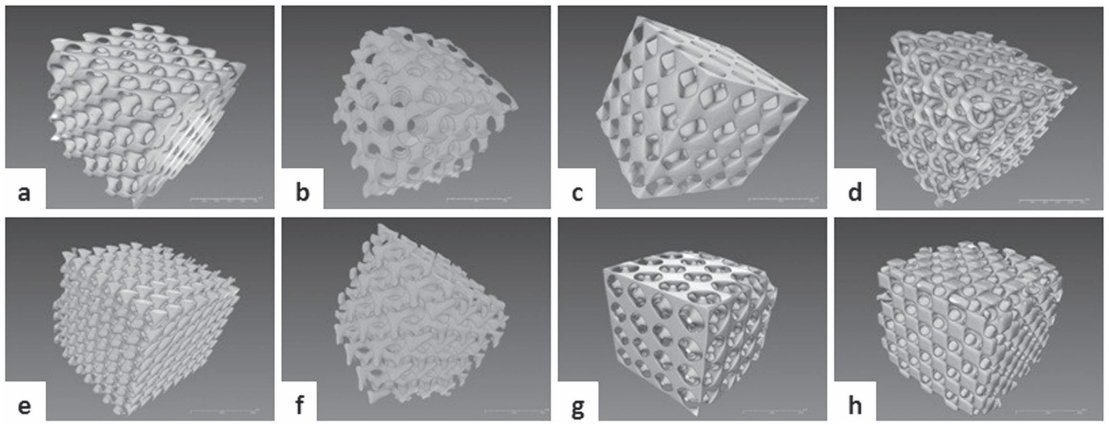

Figure 5. μCT reconstruction of the eight TPMS scaffolds based on PTMC: (a) Diamond (D); (b) Gyroid (G); (c) Schwarz P (P); (d) Fischer–Koch S (S); (e) Double Diamond (DD); (f) Double Gyroid (DG); (g) Double Schwarz P (DP); (h) F-RD.

Characterization of built scaffolds with TPMS structures

All designed TPMS structures were successfully built by SL using PTMC macromer. Using a stiffer material such as PDLLA macromer (see supplementary information), the TPMS scaffolds were built with the same efficiency (data not shown), indicating the versatility of this fabrication technology. Representative SEM images of the TPMS structures made of PTMC show the remarkable resolution of the manufacturing process, with a precise reproduction of the curved surfaces (figure 4).

The complex internal 3D structure of the scaffolds was investigated at high spatial resolution by μCT analysis (figure 5). Moreover, this technique offers insight in the accuracy of SL fabrication, which was found to be around 94%–98% for the PTMC built scaffolds with respect to the CAD design (table 3).

The μCT reconstructions of the fabricated scaffolds show homogeneous and highly interconnected pores.

As expected, the scaffolds with DD, DG and DP architectures show perfect interpenetration of each respective simple D, G and P geometry. The tortuous and intertwined architectures of the scaffolds present in figures 4(d)–(h) and 5(d)–(h) are clearly visible. By contrast, the pore geometries of D, G and P scaffolds are notably straightly open from one side of the scaffold to the other, and therefore affect substantially the specific surface area determined by μCT and reported in table 4, compared to the other geometries much more intertwined.

The table 4 reports the pore characteristics of the scaffolds measured by μCT, in terms of pore size and strut thickness which defines the material thickness from edge to edge. These measurements correspond to

Table 3. Reproducibility of the fabrication calculated from the porosity (in %) determined by μCT for the designed and built TPMS scaffolds based on PTMC.

TPMS structures	DD	S	F-RD	DG	DP	D	G	P
Porosity of designed scaffolds (%)	65.3	64.6	65.3	65.2	64.7	65.4	65	65.3
Porosity of built scaffolds (%)	61.2	62.1	61.7	66.4	60.9	64.5	66.4	66.7
Reproducibility	93.7%	96.1%	94.5%	98.1%	94.1%	98.6%	97.9%	98%

Table 4. Specific surface area (SSA), mean pore size and strut thickness for the designed and built TPMS scaffolds based on PTMC, determined by μCT.

TPMS structures	SSA of built scaffolds (mm^{-1})	SSA of designed scaffolds (mm^{-1})	Mean pore size of built scaffold (μm)	Mean pore size of designed scaffold (μm)	Mean strut thickness of built scaffold (μm)	Mean strut thickness of designed scaffold (μm)
DD	7.40	8.08	545 ± 256	578 ± 63	678 ± 138	616 ± 133
S	5.90	7.40	720 ± 132	750 ± 105	619 ± 131	529 ± 129
F-RD	5.96	6.34	1001 ± 328	1117 ± 256	964 ± 318	850 ± 306
DG	5.45	6.55	878 ± 333	700 ± 110	589 ± 76	541 ± 57
DP	4.53	5.56	818 ± 333	830 ± 125	1240 ± 440	1103 ± 420
D	4.55	5.30	1205 ± 180	1185 ± 147	854 ± 144	797 ± 158
G	3.94	4.42	1445 ± 240	1467 ± 189	881 ± 104	827 ± 132
P	3.69	4.02	2069 ± 481	2069 ± 457	1384 ± 498	1260 ± 547

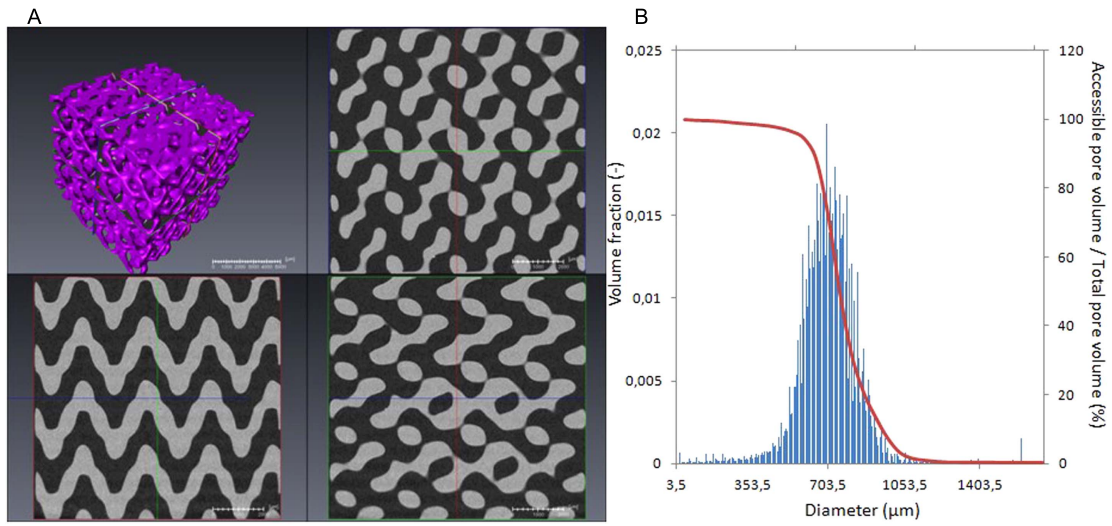

Figure 6. μCT imaging and pore interconnectivity of a built PTMC scaffold with Fischer–Koch S architecture. (A) μCT reconstruction in 3D and 2D cross-sections through different parts of the scaffold. (B) The red curve represents the pore volume that is accessible for simulated spheres of different diameters permeating through the scaffold. The histogram shows the accessible fraction of the total pore volume related to the diameter of the simulated permeating sphere. Scale bars represent 1 mm.

the diameter of a simulated permeating sphere inside the pore or inside the material [17, 38]. The same approach was used to measure the pore characteristics of the designed scaffolds. These data confirm the high precision of the fabrication method, which is around 92% as compared to the designed scaffolds.

It is important to notice that this method of calculation take only into account the accessible volume in the void or material interface and therefore neglect the surface topography. Indeed, TPMS architectures are defined from their surface topography and it seems relevant to also calculate a radius of curvature which will concretely consider the surface architecture. Thus, we propose in this article to change the vision of the pore features by introducing a new approach and method to calculate the radius of surface curvature from the calculated curvature and the equation (2). The two approaches are undeniably distinct and give two complementary indications on the pore features.

Pore interconnectivity of the built TPMS scaffold

μCT analysis was also used to determine the interconnectivity of the pores in the TPMS scaffolds using an algorithm that mimics mercury porosimetry. Figure 6(A) shows a μCT reconstruction of a scaffold with Fischer–Koch S architecture, as well as three different cross-sections through the scaffold. It clearly shows the reproduction of the S architecture with a

completely open internal structure of the scaffold. Figure 6(B) describes the interconnectivity of the void space in the Fischer–Koch S scaffold, based on the accessible pore volume for simulated spheres of different diameters permeating through the scaffold [17]. The graph shows that the interconnectivity of the pores in this scaffold is 100%. This specific interconnectivity of the pores was found for all TPMS structures investigated.

Water permeability measured with built TPMS scaffolds

The intrinsic water permeabilities of the TPMS scaffolds as determined according to Darcy's law are reported in table 5. As the porosity of each scaffold is constant (65% of porosity with 94%–98% of reproducibility, table 3), the evolution of the permeability for each scaffold cannot be modulated by the porosity. The highest intrinsic permeabilities were found for the scaffolds with the pore channel architectures (D, G and P). Moreover, the data show that the intrinsic water permeability is inversely related to the specific surface area, and thus the complexity of the inner structure of the scaffold, ranging from 7.34 mm^{-1} for the DD to 3.69 mm^{-1} for the P scaffold (see also table 4).

Discussion

To advance the field of regenerative medicine, tissue engineering scaffolds with precise and optimized properties are needed to induce effective tissue regeneration. With respect to scaffold architecture, TPMS scaffolds might be very useful as they present geometries based on the principle of minimal surfaces. Our approach combining SL, degradable polymers and TPMS-based scaffold designs, allows building scaffolds with specific optimized geometry and therefore targeting the regeneration of a wide variety of tissues.

It was shown before that cell morphology, migration behavior, stem cell fate and local tissue formation can be affected by surface curvature in the range of curvatures larger than cell size [1–4, 39]. Therefore, in addition to conventional properties like surface chemistry and stiffness, which affect cell behavior, also surface curvature must be taken into account as design parameter for advanced tissue engineering scaffolds.

TPMS architectures can be described by trigonometric equations, which allow drawing up a library of different architectures all based on minimal surfaces. TPMS scaffolds display specific functionalities such as pore interconnectivity and a periodic surface curvature distribution that may be of considerable benefit in tissue engineering. Each TPMS architecture presents a specific and periodic surface curvature distribution that can be tuned to the target tissue. The surface curvature of TPMS scaffolds has never been described in the literature, and we especially focused our study on this original functional parameter for 3D scaffolds. The surface curvature, and therefore the pore characteristics of a specific TPMS scaffold, can be easily modulated by varying the number of unit cells (n) and/or the length of the cubic side (m) of the scaffold. The maximum Gaussian curvatures calculated using equation (3) allow predicting the surface curvature of TPMS scaffolds and to potentially tailor cell behavior. Indeed, surface curvature gives a much more relevant indication on pore characteristics and surface topography, especially required in tissue engineering as cell function and behavior depend principally on the scaffold surface features. By our approach, we proposed to orient the focus on surface curvature supported by the TPMS family architecture, and we proposed a method to calculate the surface curvature distribution which can be easily modulated for specific applications.

The Gaussian curvature distributions of the eight investigated TPMS structures are not uniform (figure 2). The intrinsic complexity of the DD, S and F-RD structures leads to a broader curvature distribution with the highest surface curvature values, while D, G, P, DG and DP structures have a more narrow distribution with the lowest values for the surface curvature. Surface curvature distribution could be a useful variable in the development of co-culture systems, in which specific cell types differentially respond to low or high surface curvatures. The different equations given in table 1 require the use of a constant (C), which was chosen to keep the porosity of the scaffolds constant (65%). Changing this constant will have different effects on each structure. More precisely, this constant defines the amount of material placed around the structure skeleton. Changing of the constant leads to differences in shape, density and consequently surface curvature of each structure.

The mathematical determination of the surface curvatures revealed that the structures have not only different mean curvatures but also different curvature distributions, which vary from narrow to relatively wide. This opens the possibility to change the properties of the structures, which may be crucial for the creation of cell-supporting scaffolds since cells appear to be affected by the local surface curvature. An interesting option would be to study the effect of scaffolds with narrow curvature distributions compared with scaffold architectures with wider curvature distributions on cell behavior and tissue formation. It can be hypothesized that surface curvature with the smoother distribution might favor a homogeneous tissue reconstruction, whereas the more inhomogeneous surfaces in terms of curvature might favor cell differentiation and may be used for the replacement of more complex tissues.

The permeability of a scaffold for a fluid describes the scaffold structure independent of the sample size and fluid used, and is determined by a number of parameters including porosity, pore size, pore orientation and pore interconnectivity [40]. Permeability is also

Table 5. Intrinsic permeabilities of the eight TPMS scaffolds based on PTMC.

TPMS scaffolds	DD	S	F-RD	DG	DP	D	G	P
Permeability $\times 10^{-9}(m^2)$	2.81 $\pm$ 0.24	3.31 $\pm$ 0.18	4.11 $\pm$ 0.41	4.20 $\pm$ 0.11	4.59 $\pm$ 0.16	4.72 $\pm$ 0.35	5.59 $\pm$ 0.65	6.44 $\pm$ 0.37

related to the fluid flow in the scaffold. Fluid flow mediated shear stress is recognized to strongly influence parameters such as cell function [41, 42] and cell distribution after perfusion seeding [43], and may therefore be important as bioreactor design parameter [44, 45].

Relationships between permeability and porosity and permeability and pore size have been described in the literature [46, 47]. The complete pore interconnectivity of the TPMS scaffolds contributed to relatively high water permeabilities in the order of 10^{-9} m^2, providing an environment through which nutrients and metabolic wastes are able to diffuse, which is a prerequisite for homogeneous tissue growth [48–50]. As expected, the highest water permeabilities were found for the scaffolds with the most open pore architecture (D, G and P). Moreover, the permeability was inversely related to the specific surface area and thus the total surface area of the scaffolds, in agreement with data reported by Jung and Torquato [51]. This can be explained by increasing friction, impeding fluid flow with increasing surface area. Determination of the scaffold permeability may allow to predict mass transport under dynamic conditions in a bioreactor [52], cell differentiation [33, 46] as well as degradation kinetics of the material [53].

In summary, the fabrication of 3D scaffolds based on TPMS architectures with specific and controlled surface curvatures offers exciting new functionalities in the field of tissue engineering. This approach allows to create a library of mathematically designed scaffolds with heterogeneous zonal features by combining different TPMS architectures. This provides great potential for regeneration of anisotropic tissues such as osteochondral bone and the intervertebral disc. The next step is to investigate the effects of different TPMS architectures on cell behavior in 3D.

Conclusions

A series of eight scaffolds with mathematically defined TPMS architectures were produced by SL using the biocompatible, degradable and rubber-like material PTMC. For the first time, we report on the potential of surface curvature as distinct design parameter for advanced tissue engineering scaffolds. An equation method to determine the surface curvature of TPMS scaffolds has been developed, which allows tailoring of the scaffolds to a desired surface curvature, which potentially has an effect on cell behavior. By means of this new approach, the pore characteristics of tissue engineering scaffolds can be precisely defined. In addition to the surface curvature, the different TPMS architectures exhibit distinct specific surface areas and permeabilities, which may also influence tissue formation. Finally, we highlighted the potential benefits of TPMS architectures and their specific surface curvatures on tissue engineering applications, but they may also be of importance in many other applications such as the science of fluid adsorption or for heterogeneous catalysis devices.

Acknowledgments

We thank Frédéric Fernandez from the platform of electronic microscopy at the University of Montpellier for the SEM analyses.

References

[1] Bidan C M, Kommareddy K P, Rumpler M, Kollmannsberger P, Fratzl P and Dunlop J W C 2013 Geometry as a factor for tissue growth: towards shape optimization of tissue engineering scaffolds *Adv. Healthcare Mater.* **2** 186–94

[2] Rumpler M, Woesz A, Dunlop J W C, van Dongen J T and Fratzl P 2008 The effect of geometry on three-dimensional tissue growth *J. R. Soc. Interface* **5** 1173–80

[3] Park J Y, Lee D H, Lee E J and Lee S H 2009 Study of cellular behaviors on concave and convex microstructures fabricated from elastic PDMS membranes *Lab Chip* **9** 2043–9

[4] Werner M, Blanquer S B G, Haimi S P, Korus G, Dunlop J W C, Duda G N, Grijpma D W and Peters A 2016 Surface curvature differentially regulates stem cell migration and differentiation via altered attachment morphology and nuclear deformation *Adv. Sci.* **4** 1600347

[5] Song K H, Park S J, Kim D S and Doh J 2015 Sinusoidal wavy surfaces for curvature-guided migration of T lymphocytes *Biomaterials* **51** 151–60

[6] Cook R J and Shore B W 1979 Coherent dynamics of N-Level atoms and molecules: III. Analytically soluble periodic case *Phys. Rev.* A **20** 539–44

[7] Shearman G C, Ces O, Templer R H and Seddon J M 2006 Inverse lyotropic phases of lipids and membrane curvature *J. Phys.:Condens. Mater.* **18** S1105–24

[8] Tenchov B and Koynova R 2012 Cubic phases in membrane lipids *Eur. Biophys. J. Biophys.* **41** 841–50

[9] Angelova A, Angelov B, Mutafchieva R, Lesieur S and Couvreur P 2011 Self-assembled multicompartment liquid crystalline lipid carriers for protein, peptide, and nucleic acid drug delivery *Acc. Chem. Res.* **44** 147–56

[10] Matsen M W and Bates F S 1997 Block copolymer microstructures in the intermediate-segregation regime *J. Chem. Phys.* **106** 2436–48

[11] Thomas E L, Anderson D M, Henkee C S and Hoffman D 1988 Periodic area-minimizing surfaces in block copolymers *Nature* **334** 598–601

[12] Urbas A M, Maldovan M, DeRege P and Thomas E L 2002 Bicontinuous cubic block copolymer photonic crystals *Adv. Mater.* **14** 1850–3

[13] Eriksson J C and Ljunggren S 1994 The mechanical surface-tension and stability of minimal surface-structures *J. Colloid Interface Sci.* **167** 227–31

[14] Gandy P J F, Bardhan S, Mackay A L and Klinowski J 2001 Nodal surface approximations to the P, G, D and I-WP triply periodic minimal surfaces *Chem. Phys. Lett.* **336** 187–95

[15] Mackay A L 1994 Periodic minimal-surfaces from finite-element methods *Chem. Phys. Lett.* **221** 317–21

[16] Hyde S 1997 *The Language of Shape the Role of Curvature in Condensed Matter: Physics, Chemistry and Biology* (Amsterdam: Elsevier)

[17] Melchels F P W, Bertoldi K, Gabbrielli R, Velders A H, Feijen J and Grijpma D W 2010 Mathematically defined tissue engineering scaffold architectures prepared by stereolithography *Biomaterials* **31** 6909–16

[18] Rajagopalan S and Robb R A 2006 Schwarz meets Schwann: design and fabrication of biomorphic and durataxic tissue engineering scaffolds *Med. Image Anal.* **10** 693–712

[19] Ronca A, Ambrosio L and Grijpma D W 2013 Preparation of designed poly(D,L-lactide)/nanosized hydroxyapatite composite structures by stereolithography *Acta Biomater.* **9** 5989–96
[20] Kadkhodapour J, Montazerian H and Raeisi S 2014 Investigating internal architecture effect in plastic deformation and failure for TPMS-based scaffolds using simulation methods and experimental procedure *Mater. Sci. Eng.* C **43** 587–97
[21] Kapfer S C, Hyde S T, Mecke K, Arns C H and Schroder-Turk G E 2011 Minimal surface scaffold designs for tissue engineering *Biomaterials* **32** 6875–82
[22] Olivares A L, Marshal E, Planell J A and Lacroix D 2009 Finite element study of scaffold architecture design and culture conditions for tissue engineering *Biomaterials* **30** 6142–9
[23] Shin J, Kim S, Jeong D, Lee H G, Lee D, Lim J Y and Kim J 2012 Finite element analysis of Schwarz P surface pore geometries for tissue-engineered scaffolds *Math. Probl. Eng.* (https://doi.org/10.1155/2012/694194)
[24] Yoo D J 2011 Porous scaffold design using the distance field and triply periodic minimal surface models *Biomaterials* **32** 7741–54
[25] Cooke M N, Fisher J P, Dean D, Rimnac C and Mikos A G 2003 Use of stereolithography to manufacture critical-sized 3D biodegradable scaffolds for bone ingrowth *J. Biomed. Mater. Res.* B **64** 65–9
[26] Jacobs P F 1992 *Rapid Prototyping & Manufacturing: Fundamentals of StereoLithography* (Dearborn, Michigan: Society of Manufacturing Engineers)
[27] Jacobs P F 1996 *Stereolithography and other RP&M Technologies: From Rapid Prototyping to Rapid Tooling* (Dearborn, Michigan: Society of Manufacturing Engineers)
[28] Chapanian R, Tse M Y, Pang S C and Amsden B G 2009 The role of oxidation and enzymatic hydrolysis on the *in vivo* degradation of trimethylene carbonate based photocrosslinkable elastomers *Biomaterials* **30** 295–306
[29] Gandy P J F and Klinowski J 2002 Nodal surface approximations to the zero equipotential surfaces for cubic lattices *J. Math. Chem.* **31** 1–16
[30] Schindelin J *et al* 2012 Fiji: an open-source platform for biological-image analysis *Nat. Methods* **9** 676–82
[31] Doube M, Klosowski M M, Arganda-Carreras I, Cordelieres F P, Dougherty R P, Jackson J S, Schmid B, Hutchinson J R and Shefelbine S J 2010 BoneJ free and extensible bone image analysis in imageJ *Bone* **47** 1076–9
[32] Chor M V and Li W 2007 A permeability measurement system for tissue engineering scaffolds *Meas. Sci. Technol.* **18** 208–16
[33] Pennella F, Cerino G, Massai D, Gallo D, Labate G F D, Schiavi A, Deriu M A, Audenino A and Morbiducci U 2013 A survey of methods for the evaluation of tissue engineering scaffold permeability *Ann. Biomed. Eng.* **41** 2027–41
[34] Schoen A H 1970 Infinite periodic minimal surfaces without selfintersections *NASA Technical Report TN* D-5541 Washington, DC
[35] Schoen A H 2012 Reflections concerning triply-periodic minimal surfaces *Interface Focus* **2** 658–68
[36] Colding T H and Minicozzi W P 2006 Shapes of embedded minimal surfaces *Proc. Natl Acad. Sci. USA* **103** 11106–11
[37] Schuller-Ravoo S, Feijen J and Grijpma D W 2011 Preparation of flexible and elastic poly(trimethylene carbonate) structures by stereolithography *Macromol. Biosci.* **11** 1662–71
[38] Hildebrand T and Ruegsegger P 1997 A new method for the model-independent assessment ofthickness in three-dimensional images *J. Microsc.* **185** 65–7
[39] Lo Y P, Liu Y S, Rimando M G, Ho J H C, Lin K H and Lee O K 2016 Three-dimensional spherical spatial boundary conditions differentially regulate osteogenic differentiation of mesenchymal stromal cells *Sci. Rep.* **6**
[40] O'Brien F J, Harley B A, Waller M A, Yannas I V, Gibson L J and Prendergast P J 2007 The effect of pore size on permeability and cell attachment in collagen scaffolds for tissue engineering *Technol. Health Care* **15** 3–17
[41] Bancroft G N, Sikavitsast V I, van den Dolder J, Sheffield T L, Ambrose C G, Jansen J A and Mikos A G 2002 Fluid flow increases mineralized matrix deposition in 3D perfusion culture of marrow stromal osteloblasts in a dose-dependent manner *Proc. Natl Acad. Sci. USA* **99** 12600–5
[42] Raimondi M T, Boschetti F, Falcone L, Fiore G B, Remuzzi A, Marinoni E, Marazzi M and Pietrabissa R 2002 Mechanobiology of engineered cartilage cultured under a quantified fluid-dynamic environment *Biomech. Model. Mechanobiol.* **1** 69–82
[43] Cartmell S H, Porter B D, Garcia A J and Guldberg R E 2003 Effects of medium perfusion rate on cell-seeded three-dimensional bone constructs *in vitro Tissue Eng.* **9** 1197–203
[44] Maes F, Ransbeeck P, Van Oosterwyck H and Verdonck P 2009 Modeling fluid flow through irregular scaffolds for perfusion bioreactors *Biotechnol. Bioeng.* **103** 621–30
[45] Porter B, Zauel R, Stockman H, Guldberg R and Fyhrie D 2005 3D computational modeling of media flow through scaffolds in a perfusion bioreactor *J. Biomech.* **38** 543–9
[46] Dias M R, Fernandes P R, Guedes J M and Hollister S J 2012 Permeability analysis of scaffolds for bone tissue engineering *J. Biomech.* **45** 938–44
[47] Li J P, de Wijn J R, van Blitterswijk C A and de Groot K 2010 The effect of scaffold architecture on properties of direct 3D fiber deposition of porous Ti6Al4V for orthopedic implants *J. Biomed. Mater. Res.* A **92** 33–42
[48] Hou Q P, Grijpma D W and Feijen J 2003 Preparation of interconnected highly porous polymeric structures by a replication and freeze-drying process *J. Biomed. Mater. Res.* B **67B** 732–40
[49] Lu J X, Flautre B, Anselme K, Hardouin P, Gallur A, Descamps M and Thierry B 1999 Role of interconnections in porous bioceramics on bone recolonization *in vitro* and *in vivo* *J. Mater. Sci., Mater.* M **10** 111–20
[50] Moore M J, Jabbari E, Ritman E L, Lu L C, Currier B L, Windebank A J and Yaszemski M J 2004 Quantitative analysis of interconnectivity of porous biodegradable scaffolds with micro-computed tomography *J. Biomed. Mater. Res.* A **71A** 258–67
[51] Jung Y and Torquato S 2005 Fluid permeabilities of triply periodic minimal surfaces *Phys. Rev.* E **72** 056319
[52] Coletti F, Macchietto S and Elvassore N 2006 Mathematical modeling of three-dimensional cell cultures in perfusion bioreactors *Ind. Eng. Chem. Res.* **45** 8158–69
[53] Agrawal C M, McKinney J S, Lanctot D and Athanasiou K A 2000 Effects of fluid flow on the *in vitro* degradation kinetics of biodegradable scaffolds for tissue engineering *Biomaterials* **21** 2443–52